Metallurgical and Materials Transactions A (2015).
DOI: http://dx.doi.org/10.1007/s11661-015-2919-z

Study and Suppression of the Microstructural Anisotropy Generated During the Consolidation of a Carbonyl Iron Powder by Field-Assisted Hot Pressing

ANDREA GARCÍA-JUNCEDA[1,*], LAURA ACEBO[1], and JOSÉ MANUEL TORRALBA[1,2]

[1]IMDEA Materials Institute, Calle Eric Kandel 2, 28906 Getafe, Madrid, Spain.
[2]Universidad Carlos III Madrid, Av. Universidad 30, 28911 Leganés, Madrid, Spain.
[*]Contact e-mail: andrea.garcia.junceda@imdea.org

A spherical carbonyl iron powder was consolidated by the field-assisted hot pressing technique using graphite tools at two different temperatures, both above the austenitizing temperature. The microstructures obtained exhibited a compositional gradient in carbon along the consolidated material. Thus, the outer rim of the cylindrical samples was composed of cementite and pearlite that gradually turned to pearlite, leading to a fully ferritic microstructure at the core of the sample. The increase in the temperature has led to a higher introduction of carbon within the sample. The interposition of a thin tungsten foil between the graphite die/punches and the powders has significantly reduced the diffusion of the carbon through the iron matrix and has suppressed the microstructural anisotropy.

I. INTRODUCTION

IN the last decade, powder consolidation methods using electric current and applied external pressure have been widely investigated due to their possibility of sintering a large range of materials, including ceramics, metals, and composites, in short processing times and few processing steps, with reasonably high densities and avoiding undesirable grain growths.[1–5] In addition, the influence of the sintering parameters on the quality and mechanical properties of final iron-based consolidated materials has been extensively studied.[6–8]

In this framework, the field-assisted hot pressing (FAHP) technique is situated, in which a high densification is performed by the simultaneous application of an uniaxial pressure and a low voltage and high alternate current to the sample.[9,10] This method produces a fast generation of internal heat by Joule effect and accelerates the diffusion among iron atoms, which increases the kinetics of sintering.[11,12] The heating rate and the obtained densification are high, leading to the final consolidated sample in around 20 minutes. The powders are poured into an assembly of graphite tools, composed of several spacers, a cylindrical die, and two cylindrical punches to transmit the load. One of the limitations found in the electric current-activated/assisted sintering techniques arises in applications where high purity of the final consolidated specimens is needed, since the set-up formed by the graphite tools could lead to the introduction of carbon inside the sample during sintering at elevated temperatures and using high heating rates.[13–15] Therefore, the carbon introduction may be an undesirable effect in many applications where the presence of carbon and/or carbides in the consolidated material is detrimental to its properties. Thus, finding a way to decrease or even suppress, this contamination would be an important key issue for future processing routes of advanced novel sintered materials.

This investigation aims to provide a better understanding of the existence of a carbon contamination coming from the graphite die and graphite punches typically used for the sintering by field-assisted activated sintering techniques. The paper focuses on the effect of carbon diffusion on the microstructure of the consolidated material. Moreover, the alternative of interposing a thin tungsten foil between the powders and the die/punches has been evaluated in order to reduce or avoid the carbon contamination.

II. EXPERIMENTAL PROCEDURE

A spherical carbonyl iron powder supplied by ECKA Granules was employed in this investigation due to its low content in carbon and other interstitial elements, as shown in Table I. The powder size distribution was determined using a particle size analyzer model Malvern Mastersizer 2000 and performing three automatic measurements. The carbonyl iron powder was consolidated by FAHP in a Gleeble 3800 thermal-simulation equipment developed by Dynamic System Inc., USA. The powder was poured into a cylindrical graphite die (18 mm in diameter) and heated in a vacuum chamber (10^{-3} Pa). The heating rate to reach the two temperatures of consolidation investigated, 1273 K and 1373 K (1000 °C and 1100 °C), was 100 K/min (100 °C/

min) in both cases, with a holding time of 10 minutes followed by furnace cooling. The temperature was registered during the entire processing using three K type thermocouples, inserted 3 mm in the graphite punches and located 2 mm above the surface of the sample in the center of the die. Initially, the graphite die was gripped at a load of 5 MPa inside the vacuum chamber and once the degassing temperature was overcome, at 873 K (600 °C), the pressure was increased to 50 MPa and maintained up to cooling. In order to study an alternative to reduce or suppress the introduction of carbon coming from the graphite tools through the sample, two more consolidation processing routes were performed changing the graphite foil (15 μm thick), usually used to avoid the attachment of the consolidated material to the die and punches, by a high purity (>99.97 pct) tungsten foil (25 μm thick). All the consolidation parameters for each processing route are listed in Table II. The consolidated samples were cylindrical specimens with 18 mm in diameter and 3 mm in length. All the examinations were performed on consolidated samples longitudinal to the compression direction. The density of the sintered specimens was measured by the Archimedes method. Microstructural studies were carried out in a Zeiss EVO MA15 scanning electron microscope (SEM). To analyze the ferritic grain size distribution in the core of the samples, electron backscatter diffraction (EBSD) patterns were obtained in a FEI Helios Nanolab 600i Field Emission Gun (FEG) equipped with and Oxford Instruments HKL NordlysNano detector. EBSD acquisitions were conducted at an accelerating voltage of 15 kV with a step size of 1 μm. The grain sizes values were calculated by the linear intercept method on inverse pole figure (IPF) maps with grain boundaries which have rotation angles above 5 deg. Specimens for SEM were ground and polished by means of standardized techniques for metallographic examination. Vickers hardness (HV) tests were performed applying a load of 0.01 kg for 10 seconds to obtain a microhardness profile through the consolidated materials.

Table I. Chemical Composition of the Carbonyl Iron Powders (in Weight Percent)

Fe	C	O	N
>99.5	0.02 to 0.10	<0.3	<0.02

III. RESULTS AND DISCUSSION

A. *Carbonyl Iron Powder Characterization*

The spherical morphology of the carbonyl iron powder is shown in the SEM micrograph of Figure 1. The graphic presenting the particle size distribution can be seen in Figure 2, where it is possible to distinguish a small fraction of particles with a distribution ranging from 40 to 110 μm, which corresponds to the randomly agglomerated powders shown in the SEM micrographs of Figure 1. The values of the particle size distribution, D_{10}, D_{50}, and D_{90}, and the average particle size are listed in Table III. These data correspond to a powder with an average particle size of 9.1 μm.

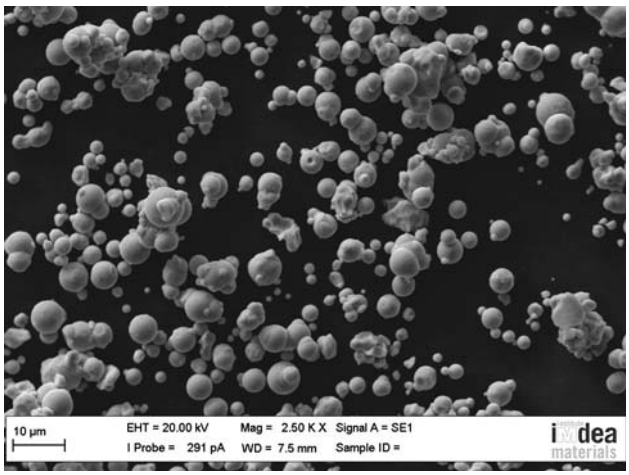

Fig. 1—Electron micrograph of the carbonyl iron powder.

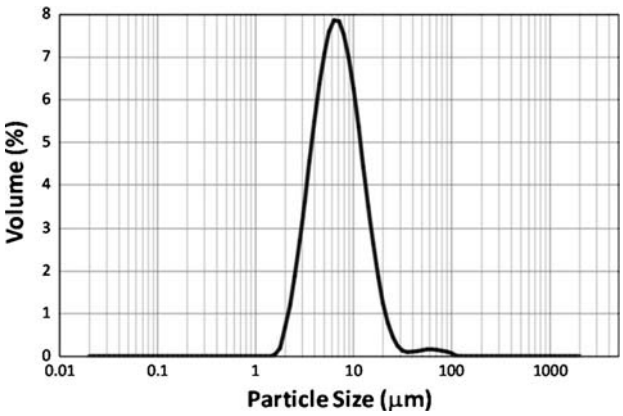

Fig. 2—Particle size distribution of the carbonyl iron powder.

Table II. Processing Route Parameters During Consolidation by FAHP

Processing Route	Heating Rate [K (°C)/min)]	Consolidation Temperature [K (°C)]	Holding Time (min)	Pressure Applied (MPa)	Type of Foil (Material)
1	100 (100)	1273 (1000)	10	50	graphite
2	100 (100)	1373 (1100)	10	50	graphite
3	100 (100)	1273 (1000)	10	50	tungsten
4	100 (100)	1373 (1100)	10	50	tungsten

Table III. Particle Size Distribution Over the Volume of the Carbonyl Iron Powder

D_{10} (μm)	D_{50} (μm)	D_{90} (μm)	Average Particle Size (μm)
3.5	7.2	15.2	9.1

B. *Consolidation by FAHP*

The carbonyl iron powder was consolidated by FAHP at the four conditions detailed in the experimental procedure epigraph. All the consolidated samples presented a density over 97 pct.

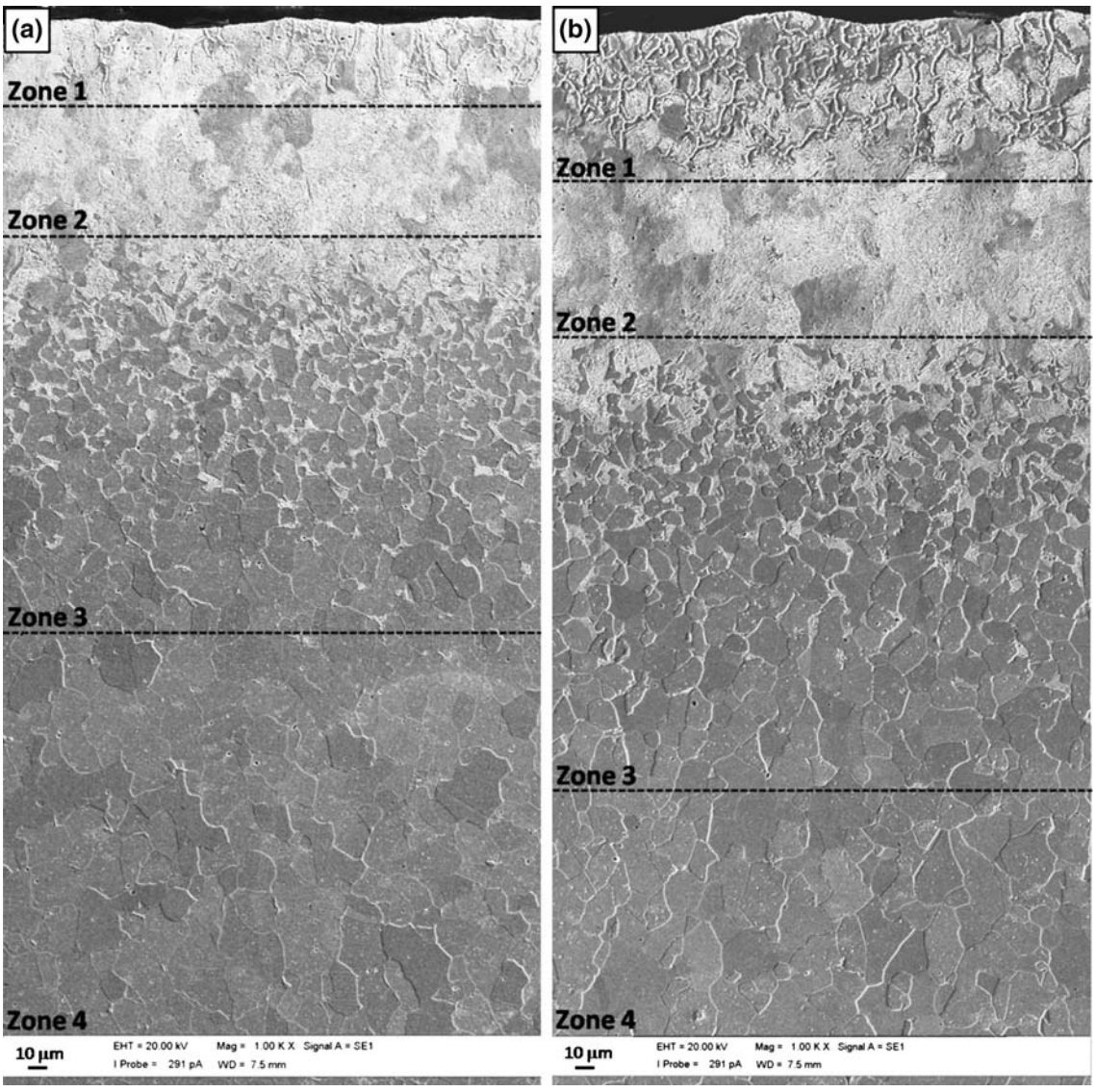

Fig. 3—Microstructure of the samples consolidated by FAHP with graphite foil: (*a*) Processing route 1 at 1273 K (1000 °C), (*b*) Processing route 2 at 1373 K (1100 °C).

Table IV. Depth Reached for Each Zone After Consolidation with Graphite Foil

Processing Route	Consolidation Temperature [K (°C)]	Zone 1 Cementite-Pearlite (μm)	Zone 2 Pearlite (μm)	Zone 3 Ferrite-Pearlite (μm)	Zone 1 + 2 + 3 (μm)
1	1273 (1000)	48	70	208	326
2	1373 (1100)	90	86	236	412

1. *Consolidation using thin graphite foils*

After the processing routes 1 and 2, carried out using the typical set-up with graphite tools and graphite foils, the obtained microstructures were heterogeneous, exhibiting a compositional gradient in the carbon content

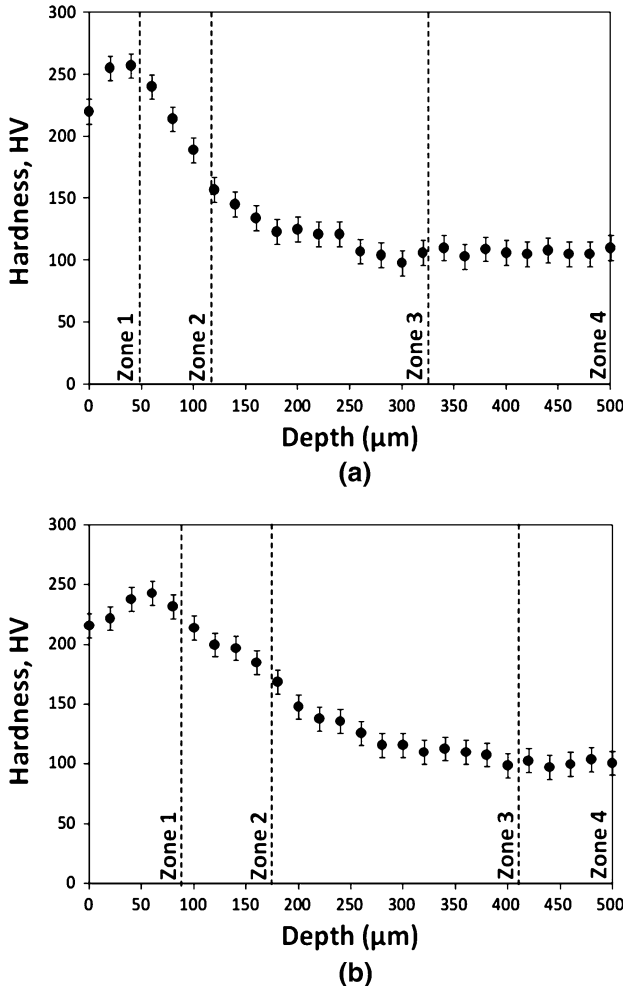

Fig. 4—Vickers microhardness depth profile in samples consolidated by FAHP with graphite foil: (*a*) Processing route 1 at 1273 K (1000 °C), (*b*) Processing route 2 at 1373 K (1100 °C).

(Figure 3). Although these electron micrographs correspond to consolidated samples longitudinal to the compression direction, it is worth mentioning that this carbon gradient was also found in the transverse direction of the consolidated samples, due to the diffusion of carbon from the die to the ferrous alloy being sintered. Due to this carbon gradient, it is possible to distinguish four different microstructural zones in the SEM micrographs of the consolidated samples. The external region that was in contact with the graphite foil is therefore enriched in carbon leading to Zone 1, which presents the typical microstructure of an hypereutectic steel, composed of lamellar pearlite (ferrite and cementite) and free cementite (Fe_3C). This region corresponds to the hypereutectoid zone of the iron-carbon equilibrium diagram.[16] These phases come from austenite with a carbon content between 0.76 and 2.14 pct in weight. However, since the carbon content within the sample is depleted with the distance, the austenite content in carbon decreases along the matrix of the consolidated material up to the eutectoid carbon content of 0.76 pct and then it transforms to pearlite, corresponding to Zone 2 of the micrographs. As a result of the continuous decrease of the carbon content along the consolidated material, the austenite carbon content decreases above the eutectoid value, entering in an hypoeutectoid area where proeutectoid ferrite is formed from austenite, in the range 1185 K to 1000 K (912 °C to 727 °C), with enrichment of the residual austenite in carbon. At 1000 K (727 °C), the remaining austenite, now with an eutectoid carbon content, transforms to pearlite producing the ferrite-pearlite region designated as Zone 3 in the SEM images. Finally, the inner part of the consolidated materials has so low carbon content (lower than 0.022 pct) that its composition is close to a pure iron and only ferrite grains are found in the matrix (Zone 4 of the micrographs). It should be noted that these ferritic grains seem to be elongated along the direction of the current application, indicating the existence of a favored grain growth in such direction. Usually, there is a textured preferential path into the perpendicular direction of the applied press (less sensible in hot processes due to the recovery and possible dynamic recrystallization), but it seems that during FAHP, the electrical current generates a texturing effect

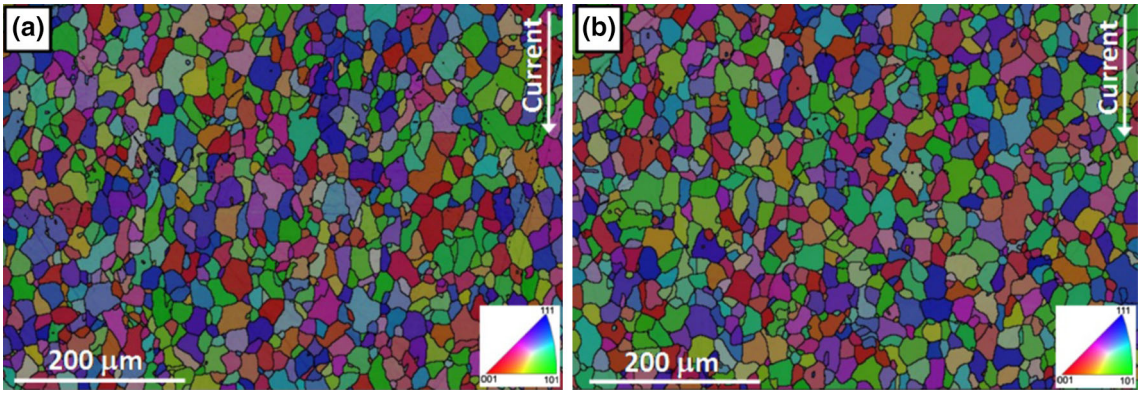

Fig. 5—Inverse pole figure maps obtained by EBSD on the core of the samples consolidated by FAHP with graphite foil: (*a*) Processing route 1 at 1273 K (1000 °C), (*b*) Processing route 2 at 1373 K (1100 °C).

in the grains producing certain elongation in the sense of the current path. All the microstructural constituents obtained correspond to the iron-carbon equilibrium diagram; metastable phases were not found, which are as a consequence of the relatively slow cooling rate at which the samples were subjected during the furnace cooling. Concerning the effect of the temperature of consolidation on the final microstructure, it is worth mentioning that the diffusion rate of carbon in iron is a function of the temperature. This dependence was firstly observed by Smith, who analyzed the diffusivity of carbon in iron[17] and was further studied by Tibbetts in steels at high temperature.[18] Thus, in this investigation, the increase of 100 K (100 °C) in the consolidation temperature has significantly increased the distance that the carbon atoms have diffused through the iron matrix of the material and, subsequently, the depth reached by the phases rich in carbon, being 326 μm at 1273 K (1000 °C) and 412 μm at 1373 K (1100 °C) (Table IV). The results of this table displaying the width of each zone as a function of the consolidation temperature (calculated from the SEM images of Figure 3) clearly point out a higher penetration of the carbon quantity coming from the graphite tools at 1373 K (1100 °C) with respect to 1273 K (1000 °C), showing a deeper extension of Zone 1 (formed by cementite-pearlite), Zone 2 (composed of

Table V. Mean Ferrite Grain Size After Consolidation with Graphite Foil (EBSD Data)

Processing Route	Consolidation Temperature [K (°C)]	Mean Length (μm)	Mean Width (μm)
1	1273 (1000)	16.4 ± 11.2	12.8 ± 8.0
2	1373 (1100)	16.7 ± 10.7	13.7 ± 8.5

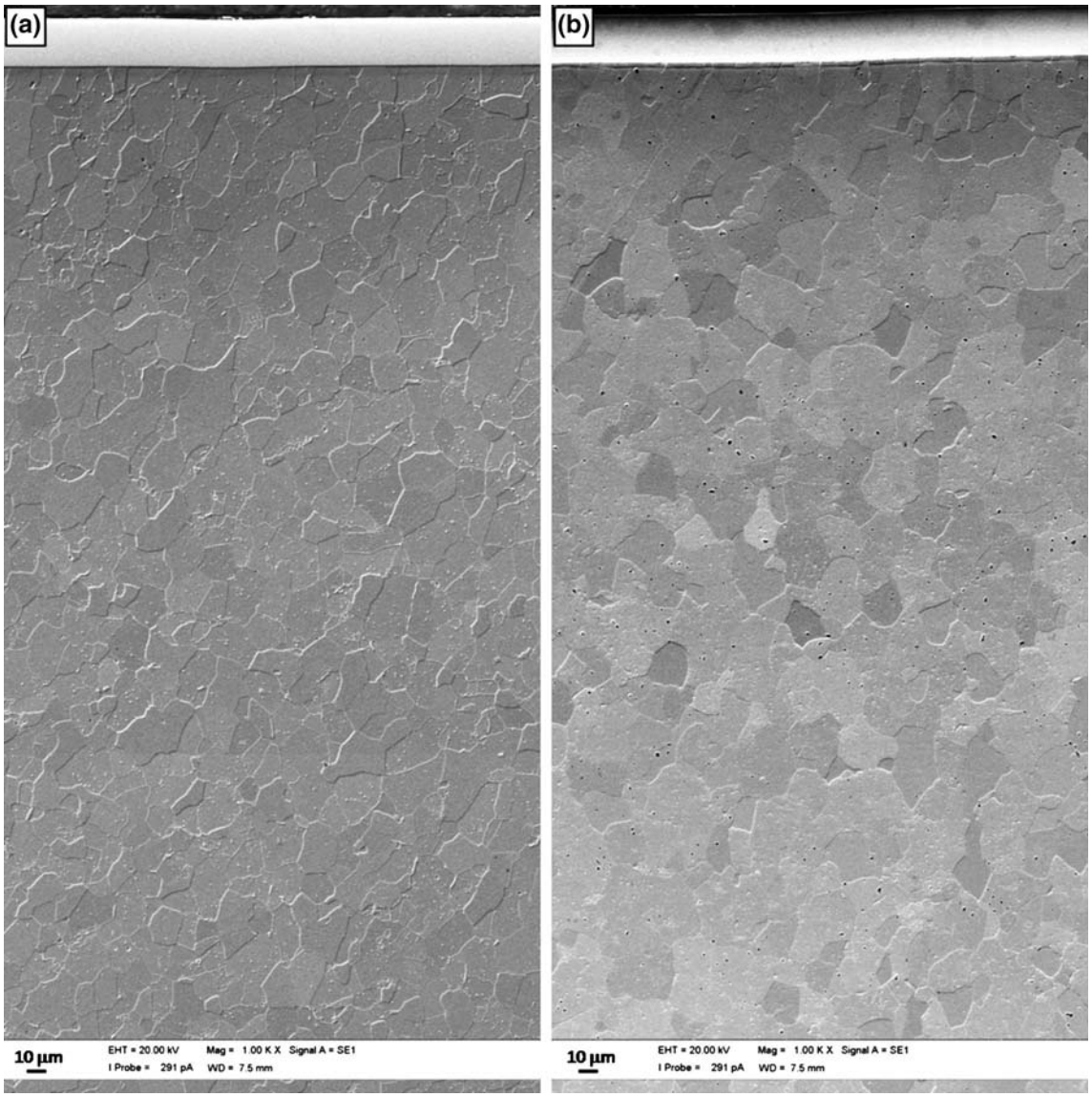

Fig. 6—Microstructure of the samples consolidated by FAHP with tungsten foil: (*a*) Processing route 3 at 1273 K (1000 °C), (*b*) Processing route 4 at 1373 K (1100 °C).

pearlite), and Zone 3 (with ferrite-pearlite). These microstructural differences through the matrix of the consolidated samples are also reflected in the microhardness depth profile values shown in Figure 4, where it is possible to distinguish the four zones previously mentioned. It should be pointed out that the hardness in the external area of both samples is around 220 HV, and

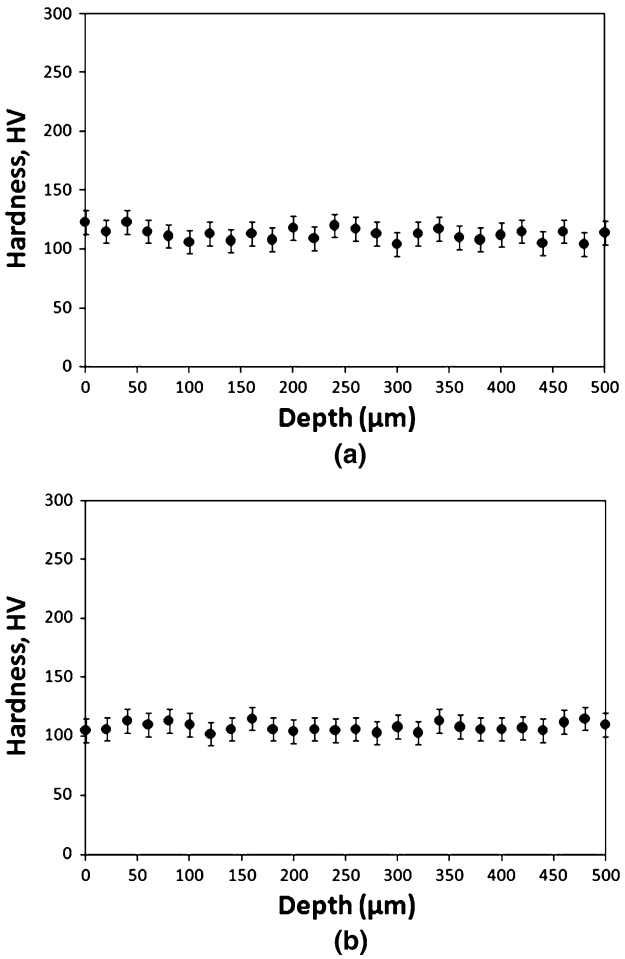

Fig. 7—Vickers microhardness depth profile in samples consolidated by FAHP with tungsten foil: (*a*) Processing route 3 at 1273 K (1000 °C), (*b*) Processing route 4 at 1373 K (1100 °C).

then it increases along Zone 1, reaching a maximum in the area composed of cementite and pearlite (245 to 255 HV). This fact is due to the mounting of the consolidated powder in a thermosetting phenolic resin (Bakelite) with a hardness value of approximately 60 HV, which decreases the value of the hardness when the test is performed near this Bakelite.[19] Furthermore, these profiles clearly show the tendency of the microhardness to decrease with the reduction in the carbon content up to a minimum value, around 100 HV for both processing routes, which remains stable along Zone 4 and corresponds to the hardness of the ferritic constituent. The study of the grain size in the core of the samples by means of EBSD data highlights the existence of a grain elongated along the direction of the current application (Figure 5), which size slightly increases with the rising of the temperature from 1273 K to 1373 K (1000 °C to 1100 °C), as shown in Table V. Since the mean ferrite grain size in the core of the specimens was similar, no significant differences were found in the hardness values corresponding to Zone 4 of both sintered samples, as detailed above. In addition, the IPF maps suggest that no texture was induced during the consolidation using the FAHP technique.

2. *Consolidation using thin tungsten foils*

Regarding the analysis of the processing routes 3 and 4, where the graphite foils were replaced by tungsten foils to evaluate the possibility of reducing or suppressing the introduction of carbon coming from the graphite die and punches, it is remarkable that the areas enriched in carbon were not found, regardless of the consolidation temperature of the route followed (Figure 6). Hence, the microstructural anisotropy has been successfully suppressed. The hardness profiles along each

Table VI. Mean Ferrite Grain Size After Consolidation with Tungsten Foil (EBSD Data)

Processing Route	Consolidation Temperature [K (°C)]	Mean Length (μm)	Mean Width (μm)
3	1273 (1000)	9.2 ± 6.0	8.6 ± 5.7
4	1373 (1100)	13.2 ± 10.1	12.6 ± 9.2

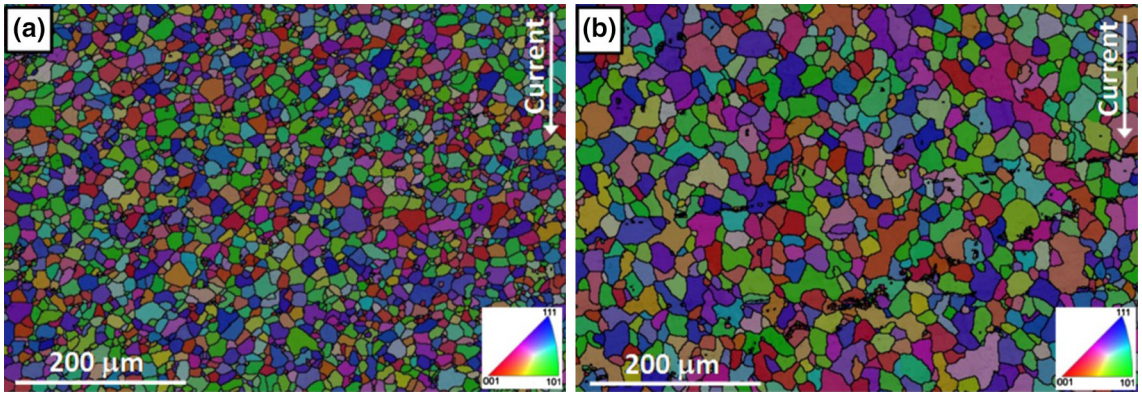

Fig. 8—Inverse pole figure maps obtained by EBSD on the core of the samples consolidated by FAHP with tungsten foil: (*a*) Processing route 3 at 1273 K (1000 °C), (*b*) Processing route 4 at 1373 K (1100 °C).

consolidated sample (Figure 7), in which no significant variations in the hardness values are presented, confirm this homogeneous ferritic microstructure. However, it is possible to observe that in the case of the sample heated up to 1273 K (1000 °C), the hardness values are slightly higher than those obtained at 1373 K (1100 °C). This hardening is probably due to the smaller grain size obtained at 1273 K (1000 °C), as expressed by the Hall–Petch relationship,[20,21] that can be clearly observed in Table VI where the mean ferrite grain size of the samples consolidated with tungsten foil obtained from EBSD data is shown. Similarly, it is observed that in the case of using a tungsten foil, the hardness of the ferritic matrix has slightly increased when comparing with the data obtained in the case of using a graphite foil. This fact may be due to the refinement of the ferritic grain size in the case of interposing a tungsten foil between the graphite tools and the powders during sintering. IPF maps in the core of the consolidated samples show again that no texture was induced in the material when sintering by means of FAHP and that the grains tend to be relatively equiaxed in the case of using tungsten foil (Figure 8). The grain growth is favored with the increase of the temperature, as expected. Although the electrical and thermal conductivities of the tungsten foil through its thickness[22] are higher than those of the graphite foil in the entire temperature range studied,[23,24] the mean ferrite grain size obtained when sintering with tungsten foils is smaller. This fact suggests that the thickness of the foil has an important effect on the grain growth rate, since a wider tungsten foil (25 *vs* 15 μm of the graphite foil) has led to a smaller and more equiaxed grain size in spite of its higher conductivity values.

IV. CONCLUSIONS

The effect of the carbon introduction on the microstructure of an iron-based alloy, consolidated by FAHP, was investigated focusing on the possibility of suggesting a way to avoid this contamination coming from the graphite die and punches used. The following conclusions were derived from the present study:

1. The use of thin graphite foils in the typical sintering set-up adopted during FAHP leads to the diffusion of carbon atoms through the iron matrix, giving rise to microstructural anisotropies in the consolidated alloy.
2. The increase of the temperature raises the depth of the areas enriched in carbon when graphite foils are used.
3. The grains are slightly elongated in the direction of the current application in the case of using graphite foils.
4. The replacement of the graphite foils, currently used in field-assisted sintering techniques, by tungsten foils of high purity inhibits the introduction of carbon in the consolidated samples and refines the final grain size.
5. The ferritic grains tend to be equiaxed in the case of using tungsten foils.
6. FAHP did not induce any texture during the processing routes analyzed in this investigation.

REFERENCES

1. M. Omori: *Mater. Sci. Eng. A*, 2000, vol. 287, pp. 183–88.
2. R. Orrù, R. Licheri, A.M. Locci, A. Cincotti, and G. Cao: *Mater. Sci. Eng. R*, 2009, vol. 63, pp. 127–287.
3. S. Grasso, Y. Sakka, and G. Maizza: *Sci. Technol. Adv. Mater.*, 2009, vol. 10, pp. 1–24.
4. D.V. Quach, J.R. Groza, A. Zavaliangos, and U. Anselmi-Tamburini: *10—Fundamentals and Applications of Field/Current Assisted Sintering: Woodhead Publishing Series in Metals and Surface Engineering*, Woodhead Publishing, Abington, 2010, pp. 249–74.
5. O. Guillon, J. González-Julian, B. Dargatz, T. Kessel, G. Schierning, J. Räthel, and M. Herrmann: *Adv. Eng. Mater.*, 2014, vol. 16, pp. 830–49.
6. S. Libardi, M. Zadra, F. Casari, and A. Molinari: *Mater. Sci. Eng. A*, 2008, vol. 478, pp. 243–50.
7. M. Pellizzari, A. Fedrizzi, and M. Zadra: *Mater. Des.*, 2011, vol. 32, pp. 1796–1805.
8. S. Pandya, K.S. Ramakrishna, A.R. Annamalai, and A. Upadhyaya: *Mater. Sci. Eng. A*, 2012, vol. 556, pp. 271–77.
9. R. Muñoz-Moreno, E.M. Ruiz-Navas, B. Srinivasarao, and J.M. Torralba: *J. Mater. Sci. Technol.*, 2014, vol. 30, pp. 1145–54.
10. B. Srinivasarao, J.M. Torralba, M.A. Jabbari Taleghani, and M.T. Pérez-Prado: *Mater. Lett.*, 2014, vol. 123, pp. 75–78.
11. K. Feng, Y. Yang, M. Hong, J. Wu, and S. Lan: *J. Mater. Process. Technol.*, 2008, vol. 208, pp. 264–69.
12. J. Räthel, M. Herrmann, and W. Beckert: *J. Eur. Ceram. Soc.*, 2009, vol. 29, pp. 1419–25.
13. G. Bernard-Granger, N. Benameur, C. Guizard, and M. Nygren: *Scripta Mater.*, 2009, vol. 60, pp. 164–67.
14. Y. Liu and Z. Jin: *Ceram. Int.*, 2012, vol. 38, pp. 217–22.
15. W. Wang, H. Kou, S. Liu, Y. Shi, J. Li, X. Feng, Y. Pan, Y. Li, and J. Guo: *Ceram. Int.*, 2015, vol. 41, pp. 2576–81.
16. H.K.D.H. Bhadeshia and R.W.K. Honeycombe: *Steels*, 3rd ed., Butterworth-Heinemann, Oxford, 2006, pp. 39–70.
17. R.P. Smith: *Acta Metall.*, 1953, vol. 1, pp. 578–87.
18. G.G. Tibbetts: *J. Appl. Phys.*, 1980, vol. 51, pp. 4813–16.
19. M. Fáberová, R. Bureš, and E. Dudrová: *Powder Metall. Prog.*, 2009, vol. 9, pp. 212–18.
20. E.O. Hall: *Proc. Phys. Soc. B.*, 1951, vol. 64, pp. 747–53.
21. N.J. Petch: *J. Iron Steel Inst.*, 1953, vol. 174, pp. 25–32.
22. E. Lassner and W.D. Schubert: *Tungsten: Properties, Chemistry, Technology of the Element, Alloys, and Chemical Compounds*, Kluwer Academic, New York, 1999.
23. A.K. Dutta: *Phys. Rev.*, 1953, vol. 90, pp. 187–92.
24. C.N. Hooker, A.R. Ubbelohde, and D.A. Young: *Proc. R. Soc. A.*, 1965, vol. 284, pp. 17–31.